Journal of Applied Polymer Science

Preparation of modified oligochitosan and evaluation of its scale inhibition and fluorescence properties

Huixin Zhang,[1] Zhiyue Cai,[1] Xiuhong Jin,[2] Dongxue Sun,[1] Dongdong Wang,[1] Tingru Yang,[1] Jie Zhang,[1] Xu Han[1]

[1]School of Chemistry and Chemical Engineering, Hebei University of Technology, Tianjin 300131, People's Republic of China
[2]Tianjin Research and Design Institute of Chemical Industry, China National Offshore Oil Corporation, People's Republic of China
Correspondence to: H. Zhang (E-mail: zhanghuixin@hebut.edu.cn)

ABSTRACT: To obtain an environmentally friendly and efficient scale inhibitor, carboxymethyl quaternary ammonium oligochitosan (CM-QAOC) was prepared from chitosan, which was depolymerized by nitrous acid, and then reacted with chloroacetic acid and glycidyl trimethyl ammonium chloride via carboxymethylation and quaternization, respectively. The chitosan derivatives were characterized by Fourier transform infrared and NMR spectroscopy. The inhibition performance for CM-QAOC was evaluated by a conductivity method and a static antiscaling test. The experiments demonstrated that CM-QAOC showed an excellent scale-inhibition performance. With a Ca^{2+} concentration of 240 mg/L, CM-QAOC at a concentration of 50 mg/L and pH 8.0 gave an antiscaling ratio of more than 98%. So, CM-QAOC could be applied as an excellent antiscaling agent. Furthermore, a detectable fluorescence of CM-QAOC solution was observed. To understand this interesting fluorescence phenomenon and to explore the probability of its being a fluorescent tracer, the relations between the fluorescence intensities and CM-QAOC concentrations and the pH influence on the fluorescence intensities were investigated. The results show the fluorescence intensities accorded well with the concentrations of CM-QAOC with a detection limit of 0.6046 mg/L, and the fluorescence intensity was constant within pH 5–9; this indicated that it had the potential of its being a fluorescent tracer. Thus, CM-QAOC could be applied as an antiscaling water-treatment chemical and as a fluorescence tracer directly without any further modifications. It could be self-traced online and in real time with its own fluorescence, although more work should be done to investigate its fluorescent mechanism and its tracing properties in detail. © 2015 Wiley Periodicals, Inc. J. Appl. Polym. Sci. **2015**, *132*, 42518.

KEYWORDS: applications; polysaccharides; spectroscopy

Received 1 December 2014; accepted 19 May 2015
DOI: 10.1002/app.42518

INTRODUCTION

In recent years, the consumption and pollution of industrial water in China has increased significantly with the rapid development of industries; this has intensified the shortage of fresh water resources.[1] To alleviate the problem, it is imperative to add a variety of water-treatment chemicals into the water systems to economize water and inhibit damages such severe corrosion and scaling.[2] A scale inhibitor is an important kind of water-treatment chemical that is generally used in industrial water systems. Phosphorus scale inhibitors are widely applied; these include phosphonates, organic phosphorus-containing polymers due to their high effectiveness,[3,4] but they cause secondary pollution and ecological imbalance in water. Therefore, the development of natural products and their modified derivatives as environmentally friendly green scale inhibitors has been drawing the great attention of scientists and researchers.[5,6]

When a kind of water-treatment chemical is used to prevent the formation of scales, the concentration of the water-treatment agent in the water system must be controlled within a prescribed range to maintain its ideal function with good efficiency. It is hoped that the concentration of water-treatment chemicals can be monitored accurately and in real time through a simple operation over time. Inert fluorescent tracers have been used to determine the amount of water-treatment chemicals in water systems.[7–9] The addition of inert fluorescent tracers should be proportional to the dosages of water-treatment chemicals. By measuring the fluorescent signals of the fluorescent tracers with a fluorometer, one can determine the concentration of the inert fluorescent tracers, and the real-time concentration of water-treatment chemicals can be traced indirectly. The advantage of fluorescent tracers is that they can be measured online and in real time so that any variation in the concentration of water-treatment chemicals can be traced immediately.[10] However, because of simple physical blending,

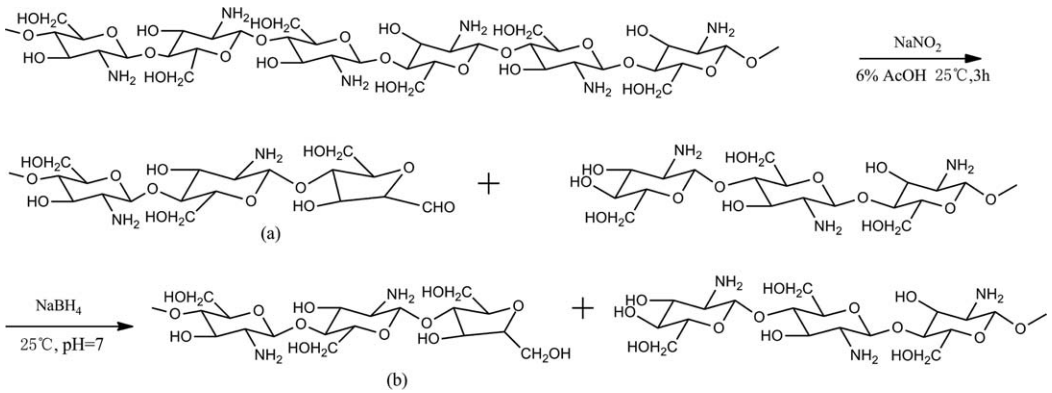

Scheme 1. Depolymerization of the chitosan by $NaNO_2$ and AcOH and subsequent reduction by $NaBH_4$.

extraneous inert fluorescent tracers can be easily separated from the water-treatment chemicals, and this leads to some errors or failures in the indication of changes in the concentration of inert fluorescent tracers and fluctuations in the dosages of water-treatment chemicals. Thus, to trace the concentration of water-treatment chemicals more reliably and accurately, the preparation of self-traced water-treatment chemicals that can produce fluorescence by themselves is a better solution.[11,12]

Chitosan is a partially *N*-deacetylated derivative of chitin, which is the second most abundant natural biopolymer and is derived from the exoskeletons of crustaceans and also from the cell walls of fungi and insects. Chitosan is an amenable molecule, and this amenable polymer can be modified by chemical methods because it provides plentiful functional groups such as —NH_2 and —OH groups in its monomers.[13] Chitosan and its derivatives have been well documented to have some advantageous characteristics, including biocompatibility, biodegradability, nontoxicity, abundancy, and low cost. As a result, chitosan and its derivatives have already been widely applied in the pharmaceutical industry, cosmetic industry, textile industry, biotechnologies, food processing, paper making, and agriculture.[14–17] Meanwhile, because of their nontoxic, biodegradable, and environmentally friendly properties, chitosan derivatives are currently being explored intensively for their applications in water and wastewater treatment, and various modified chitosans have been applied as very important water-treatment chemicals. Chitosan and crosslinked chitosan as adsorbents have displayed outstanding removal capabilities for certain metal ions.[18,19] Carboxymethyl chitosan is an amphiprotic ether derivative, which can prevent scale formation with chelation and dispersion properties.[20] Quaternized derivatives, such as *N,N,N*-trimethyl chitosan and *N*-(2-hydroxyl)-propyl-3-trimethylammonium chitosan chloride, are much more water soluble than chitosan in a much broader pH range and show markedly improved antimicrobial activities in pH-regulated environments.[21,22]

In this study, carboxymethyl quaternary ammonium oligochitosan (CM-QAOC) was successfully prepared and characterized by Fourier transform infrared (FTIR) spectroscopy and NMR. The antiscaling performances of the modified chitosan were evaluated with both the conductivity method and the static antiscaling test. Weak but detectable fluorescence of CM-QAOC was discovered. To explore its probability as a tracer for its own concentration, the relation between the concentration and fluorescence intensity of CM-QAOC was studied. Then, the effect of the pH value of the solution on the fluorescence properties of CM-QAOC was also investigated.

EXPERIMENTAL

Reagents and Instruments

Chitosan (degree of *N*-deacetylation > 95%, weight-average molecular weight = 350 kDa, determined through an Ubbelohde viscometer) was purchased from Jinan Haidebei Marine Bioengineering Co., Ltd. (China). All other reagents, purchased from Tianjin Fuchen Chemical Reagents Factory, were analytical-reagent grade and were used without further purification.

IR spectra were obtained from samples in KBr pellets at a resolution of 4.0 cm^{-1} over the range 4000–400 cm^{-1} with a Bruker Vensor 27 FTIR spectrophotometer (Bruker, Germany) with a deuterated triglycine sulfate (DTGS) detector. NMR spectra were acquired on a Bruker AV 400 spectrometer (Bruker, Switzerland). Oligochitosan (OC) was dissolved in D_2O/CH_3COOH and CM-QAOC was dissolved in D_2O as a solvent at 25°C. The morphology and crystal lattices of scale were observed with an S-4800N scanning electron microscope (Hitachi, Japan) under 3.0-kV voltages. Fluorescence spectra were collected with an F-4500 fluorescence spectrophotometer (Hitachi, Japan). Fluorescence decay was measured on an FLS920 spectrometer (Edinburgh Instruments, Germany). UV absorption spectra were measured with an Lambda 25 double-beam ultraviolet–visible (UV–vis) spectrophotometer (PerkinElmer) with deionized water as a solvent. All pH measurements were made with a model PHS-3C meter (Shanghai Rex Electric Chemical, China).

Synthesis

Degradation of Chitosan. OC was prepared by oxidative degradation with sodium nitrite ($NaNO_2$).[23] In the depolymerization, 2-amino-2-deoxy-D-glucopyranose units deaminated under nitrous acid's attack to form reducing 2,5-anhydro-D-mannose units, which were unstable (Scheme 1). To obtain a stable OC, a reductive agent, sodium borohydride ($NaBH_4$), was used to reduce the 2,5-anhydro-D-mannose units with the resulting product 2,5-anhydro-D-mannitol in this study. In a typical method, a solution of $NaNO_2$ (0.2571 g in 10 mL of water) was added dropwise to a solution of chitosan [3.0 g in 100 mL of 6% aqueous acetic acid (AcOH)] with constant stirring for 0.5 h. The reaction mixture was stirred for an additional 2.5 h

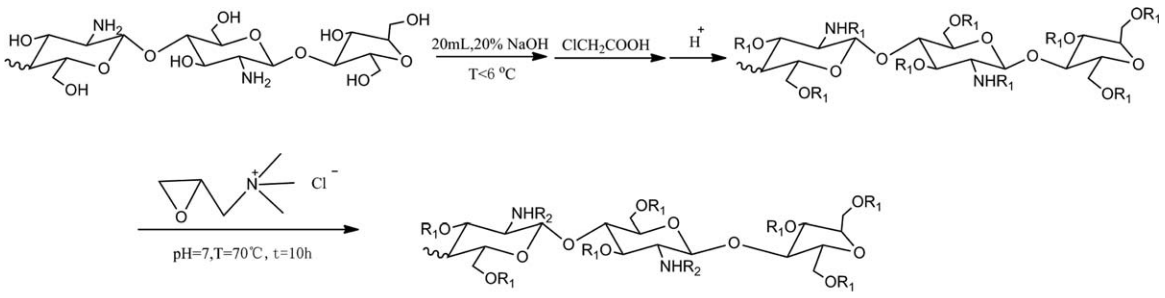

R_1=H, CH_2COOH
R_2=H,CH_2COOH, $CH_2CH(OH)CH_2N(CH_3)_3Cl$

Scheme 2. Synthetic route for CM-QAOC.

at room temperature; then, the pH was adjusted with a sodium hydroxide (NaOH) solution (4 mol/L) to pH 7–8. To the resulting mixture, portions of $NaBH_4$ (total = 0.2828 g) were added with the temperature maintained at less than 10°C. After the addition of $NaBH_4$, the solution was stirred overnight at room temperature. The white yellowish solid was recovered by centrifugation, washed several times with ethanol (80%), and dried overnight *in vacuo* at 40°C. The obtained OC was characterized by FTIR spectroscopy and ^{1}H-NMR. The molecular weight of the resulting OC was determined by the viscosity method. The characteristic viscosity [η] of the OC solution was recorded at a temperature of 25 ± 0.1°C in a mixing solvent of AcOH and NaCl (0.1 : 0.2 mol/L). The viscosity-average molecular weight (M_v) was calculated with the Mark–Houwink equation:

$$[\eta] = KM_v^{\alpha}$$

where K is 1.81×10^{-3} and α is 0.93.[24] K is the parameter depended on temperature and α is the parameter related to molecule weight. In our experiment, the mean molecular weight of the degraded chitosan was about 18.3 kDa, and the intrinsic viscosity was 16.7 cm^3/g.

Preparation of CM-QAOC. Synthesis of CM-QAOC was carried out according to some previously published procedures[25,26] but with several modifications. OC (3.00 g) was dispersed in an NaOH solution (20%, 20 mL) under stirring at a low temperature ($T < 6$°C) for 2 h. Chloroacetic acid (6.0 g in 10 mL of water) was slowly added to the previous solution under stirring for 0.5 h. The reaction mixture was allowed to react for an additional 3.5 h at 60°C. The resulting solution was adjusted to pH 6–7 with glacial AcOH and poured into excess ethanol.[27] The precipitate was collected, washed with ethanol (80%), and dried *in vacuo* at 40°C to obtain carboxymethyl oligochitosan (CMOC).

CMOC (0.5 g) was dissolved in 10 mL of H_2O. Glycidyl trimethyl ammonium chloride (1.41 g in 10 mL of water) was dropped into the previous solution in two portions within a 1-h interval. The reaction was carried out for 8 h at 80°C. After the reaction, the clear yellowish liquor was poured into an acetone/ethanol (1/1 v/v) mixture and left overnight in a refrigerator.[27] The precipitate was collected and dried *in vacuo* at 50°C to obtain a pale yellow product, CM-QAOC, and then characterized by FTIR spectroscopy and NMR. According to the viscosity method mentioned in the Degradation of Chitosan section, the intrinsic viscosity of CM-QAOC was 11.9 cm^3/g, and the mean molecular weight of CM-QAOC was approximately 12.7 kDa, as estimated. The synthetic route to CM-QAOC is shown in Scheme 2.

Determination of the Degree of Substitution. The degree of substitution of NH_2 or OH groups in OC with the carboxyalkyl group (DSC) was determined by potentiometric titration.[28] DSC was calculated as follows:

$$\mathrm{DSC} = \frac{0.203 \times (V_{2,\mathrm{NaOH}} - V_{1,\mathrm{NaOH}}) \times (C_{\mathrm{NaOH}}/m)}{1 - 0.058 \times (V_{2,\mathrm{NaOH}} - V_{1,\mathrm{NaOH}}) \times (C_{\mathrm{NaOH}}/m)} \quad (1)$$

where C_{NaOH} is the concentration of NaOH solution (mol/L), $V_{2,NaOH}$ is the volume of NaOH consumed by redundant HCl and —COOH (mL), $V_{1,NaOH}$ is the volume of NaOH consumed by redundant HCl (mL), and m is the weight of CMOC (g).

The chlorine content in CM-QAOC was measured by an $AgNO_3$ titration method to determine the degree of substitution of NH_2 groups in OC with the quaternary ammonium group (DSQ).[29] DSQ was calculated as follows:

$$\mathrm{DSQ} = \frac{(V_{1,AgNO_3} - V_{0,AgNO_3}) \times C/1000}{(V_{1,AgNO_3} - V_{0,AgNO_3}) \times C/1000 + \{W - [(V_{1,AgNO_3} - V_{0,AgNO_3}) \times C \times M_2/1000]\}/M_1} \quad (2)$$

where C is the concentration of $AgNO_3$ standard solution (mol/L), $V_{1,AgNO3}$ is the volume of $AgNO_3$ solution consumed by CM-QAOC solution (mL), $V_{0,AgNO3}$ is the volume of $AgNO_3$ solution consumed in the blank test (mL), W is the weight of CM-QAOC (g), M_1 is the molar mass of CMOC (g/mol), and M_2 is the molar mass of CM-QAOC (g/mol).

Evaluation of the Scale Inhibition Performances

Evaluation of the Scale Inhibition Performances by the Conductivity Method. The conductivity method[30,31] was carried out with the following procedure: 44 mL of distilled water, $CaCl_2$ solution (1.0 mL, 0.1000 mol/L), and a variable amount of scale inhibitor were added to a 100-mL, three-necked flask under stirring. Then, the flask was placed in a thermostatic water bath at 30 ± 0.1°C. The solution was titrated with Na_2CO_3 solution (0.1000 mol/L). The titration solution was added slowly, and the conductivity value was recorded. The conductivity was proportional to the titer of the titrating agent; thus, the initial point when scaling began to precipitate could be determined by the conductivity value. The *degree of supersaturation* (S), which is defined as the ratio of the concentration of crystallized product to the concentration of saturated product, was calculated on the basis of the following equation:

$$S = \left[Ca^{2+}\right] \cdot \left[CO_3^{2-}\right] / K_{sp}(CaCO_3) \quad (3)$$

where $[Ca^{2+}]$ and $[CO_3^{2-}]$ are the individual calcium and carbonate ion concentrations when turbidity first occurs (mol/L) and $K_{sp}(CaCO_3)$ is the ionic product of $CaCO_3$.

The S values with a scale inhibitor present were compared to those with the scale inhibitor absent under similar conditions. So the relative degree of supersaturation values (S_r) are expressed as ratios of the supersaturation values of $CaCO_3$ in the presence of a scale inhibitor (S_p) to the supersaturation value in the absence of a scale inhibitor (S_0) under the same conditions:

$$S_r = \frac{S_p}{S_0} \quad (4)$$

Antiscaling Evaluation of CM-QAOC by the Static Antiscaling Inhibition Test. The scale inhibition efficiency was determined with static antiscaling measurement in light of GB/T 16632-2008 (China) clauses. The process is as follows. Several equal portions of 0.1000 mol/L calcium chloride standard solution were placed into a set of 250-mL volumetric flasks and then diluted to 100 mL with deionized water. The scale inhibitor solution (0.5 g/L) was added to each of the previous dilutions in doses, and these were subsequently shaken well. The pH values of these solutions were adjusted to their setting points with a borax buffer solution. At last, the bicarbonate standard stock solution (0.1000 mol/L) was rationed *pro rata* with a ratio of 2 : 1 mol/mol to Ca^{2+} under shaking via a burette. The mixture solutions were diluted to 250 mL with distilled water, shaken to ensure sufficient mixing, then transferred into Erlenmeyer flasks, and immersed in a water bath at 50°C for 10 h. In addition, a blank experiment without scale inhibitor addition was carried out as a reference.[32]

The solutions were filtered after they were cooled to room temperature. To understand the interaction between the scale component and the inhibitor, $CaCO_3$ scales in every Erlenmeyer flask were collected and observed via scanning electron microscopy (SEM). The Ca^{2+} concentration of the filtrate was titrated with ethylene diamine tetraacetic acid (EDTA) titration. The scale inhibition ratio (η; %) of the scale inhibitor was calculated according to the following formula:

$$\eta = \frac{C_1 - C_2}{C_0 - C_2} \times 100\% \quad (5)$$

where C_1, C_2, and C_0 are the concentrations of Ca^{2+} in the test solution after incubation in the presence of scale inhibitors, in the absence of scale inhibitors, and before incubation (mg/L), respectively.

Investigation of the Fluorescence Properties

OC or CM-QAOC was dissolved first as sample and then diluted with deionized water or phosphate buffer solvent to the set concentrations. The sample solutions were finally placed in the dark to equilibrate overnight at room temperature.

Absorption spectra were recorded on a PerkinElmer Lambda 25 double-beam UV–vis spectrophotometer at a scan rate of 120 nm/min with a slit width of 1 nm. The fluorescence spectra were acquired on a Hitachi F-4500 fluorophotometer with an excitation source of a 150-W xenon arc lamp at a scanning rate of 240 nm/min, a voltage of 700 V, and a width of 10 nm for both excitation and emission slits. The fluorescence decay of the sample in 100 mg/L aqueous solution was measured on an Edinburgh Instruments FLS920 spectrometer with a nanosecond flash lamp as an excitation source, a double-excitation monochromator (1800 lines/mm), an emission monochromator (600 lines/mm), and a semiconductor-cooled Hamamatsu model RMP928 photomultiplier tube. The excitation wavelength was 250 nm, and the emission wavelength was 450 nm. The fluorescence decay was collected with a time-correlated single-photon counting method. We recorded the instrumental response function under the same conditions at the excitation wavelength by replacing the sample with a scattering solution of colloidal silica (Ludox). The fluorescence intensity decay was analyzed with the system software (F900) of an Edinburgh Instruments FLS920 spectrometer.

RESULTS AND DISCUSSION

Characterization of OC and CM-QAOC

FTIR and NMR Analysis. Figure 1 shows the FTIR spectra of raw chitosan [Figure 1(A)], OC [Figure 1(B)], CMOC [Figure 1(C)], and CM-QAOC [Figure 1(D)]. The characteristic absorptions of chitosan and OC at 3400cm^{-1} (ν_{O-H} and ν_{N-H}); 2924 cm^{-1} (ν_{C-H}); 1655, 1565, and 1384 cm^{-1} (δ_{N-H} and δ_{C-N}); 1050 and 1152 cm^{-1} (ν_{C-O-C}); 1030 and 1080 cm^{-1} (ν_{C-O}), and 895 cm^{-1} (β–δ_{C-H}) were easily identified. Compared with raw chitosan, the spectra of OC was almost unchanged except for the intensity of a few peaks. Moreover, the peak at 895 cm^{-1}, due to the end-group epimeric β–δ_{C-H}, proved that the basic structure of chitosan chains was not destroyed by the degradation process.[33] CMOC presented a strong and wide peak at 1602 cm^{-1} due to the C═O stretching peaks of COO^- and an enhanced C—O stretching band at 1074 cm^{-1}; this verified that a high carboxymethylation of OH and —O—CH_2COO^- groups had been formed.[34] In addition, the C—N stretching band at 1325 cm^{-1} became more intense, and the —NH_2 deformation vibration peak at 898 cm^{-1} weakened; this verified that *N*-carboxymethylation occurred. In the spectra of CM-QAOC, the NH_2 scissoring peak at 1599 cm^{-1} weakened, and a —CH_3 deformation vibration band at 1478 cm^{-1} appeared; this indicated that the quaternary ammonium groups were successfully grafted onto OC molecules.[35] In conclusion, from the FTIR spectroscopy, we observed that

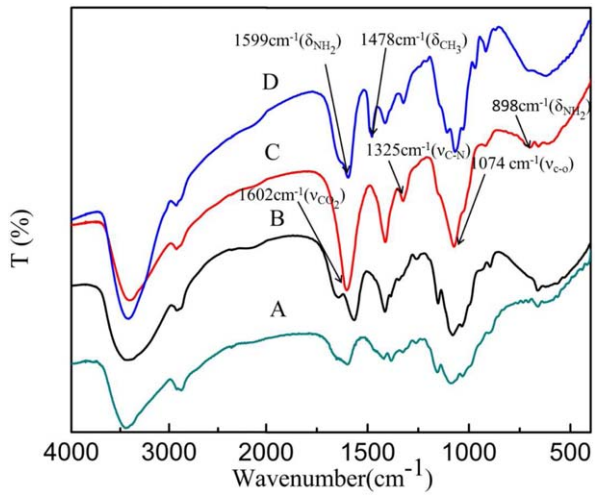

Figure 1. FTIR spectra of (A) chitosan, (B) OC, (C) CMOC, and (D) CM-QAOC. [Color figure can be viewed in the online issue, which is available at wileyonlinelibrary.com.]

carboxymethyl and quaternary ammonium groups were successfully introduced onto the OC molecules.

Figure 2(A) shows the ^{1}H-NMR spectra of OC and CM-QAOC.[27] The protons of C(1)–C(6) in the repeating units of glucosamine in CM-QAOC presented very similar chemical shifts to those shown in OC. The peaks at δ = 4.40 and 2.40 ppm were attributed to H-1 and H-2, respectively, and those at δ = 3.45–3.82 ppm were attributed to H-3 through H-6. The e-CH_2 peak at δ = 4.15 ppm indicated the carboxymethylation of OH-6 or OH-3. The a-CH_2 peak of the secondary amine, the b-CH peak, and the c-CH_2 peak were indicated at δ = 2.63–2.80 ppm, δ = 4.15–4.01 ppm, and δ = 3.27 ppm, respectively. Remarkably, there was a new intense d-CH_3 peak at δ 3.07 ppm; this indicated well the synthesis of CM-QAOC.

Figure 2(B,C) show the ^{1}H–^{1}H correlation spectroscopy (COSY) and ^{1}H-^{13}C heteronuclear single-quantum coherence (HSQC) spectral patterns of CM-QAOC. The carbon signals of δ(C) = 102.5, 78.3, 75.0, 70.3, 63.7, and 63.2 ppm, which could correlate with δ(H) = 4.40, 3.56, 3.49, 3.82, 3.45, and 2.40 ppm, respectively, were assigned to C-1, C-4, C-5, C-3, C-6, and C-2, respectively, on the repeating unit of glucosamine.[36] The correlations of δ(C) = 64.8 ppm and δ(H) = 4.15 ppm and δ(C) = 66.5 ppm and δ(H) = 4.15 ppm were assigned to the e-CH_2 of the carboxymethyl group, which substituted on OH-3 and OH-6, and the correlation of δ(C) = 54.3 ppm and δ(H) = 3.61 ppm was assigned to e-CH_2 of carboxymethyl group substituting on NH_2.[37,38] The strong signal appearing at δ(C) = 54.3 ppm and δ(H) = 3.07 ppm was assigned to d-CH_3 of the quaternary ammonium group. The δ(C) = 64.8 ppm and δ(H) = 4.15 ppm and δ(C) = 64.8 ppm and δ(H) = 4.02 ppm correlation signals were assigned to b-CH of the quaternary ammonium group, whereas the δ(C) = 51.6 ppm and δ(H) = 2.80 ppm and δ(C) = 51.6 ppm and δ(H) = 2.63 ppm signals were assigned to a-CH_2 of the secondary amine.[36] With regard to the COSY spectrum, the correlation between δ(H) = 4.40 ppm and δ(H) = 2.40 ppm confirmed that these two protons belonged to C-1 and C-2, respectively. The correlations of δ(H) = 4.15 ppm with δ(H) = 2.63 ppm and δ(H) = 3.27 ppm confirmed that the signal of protons on b-CH_2 appeared at δ(H) = 4.15 ppm. Because the e-CH_2 peak also appeared at δ(H) = 4.15 ppm, we reasonably speculated that the signals of the protons on e-CH_2 and b-CH_2 overlapped.[39]

Determination of the Degrees of Substitution. DSC and DSQ were determined by potentiometric titration and complexometric titration, respectively, and are shown in Figure 3. From the potentiometric curve in Figure 3(A-i), titration end points were determined with the second partial derivatives [Figure 3(A-ii)]. $V_{1,NaOH}$ reveals the volume of NaOH titrant consumed by

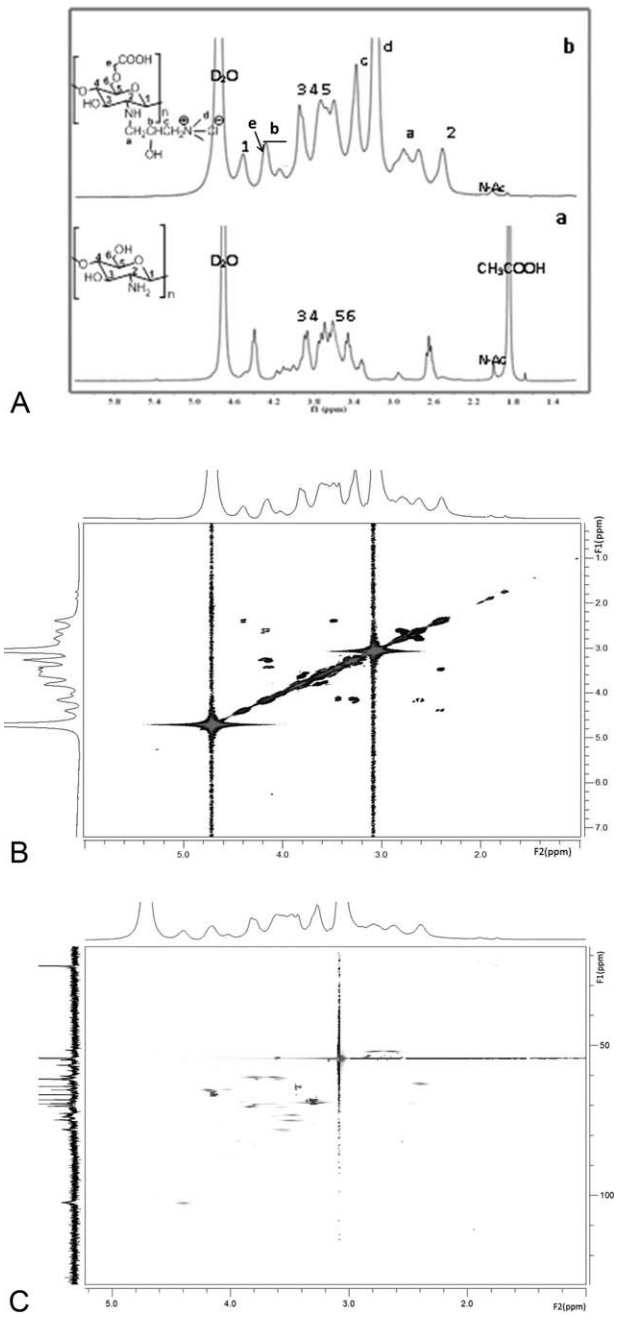

Figure 2. (A) ^{1}H-NMR spectra of (a) OC and (b) CM-QAOC, (B) H,H-COSY of CM-QAOC (F1, F2: chemical shift of ^{1}H), and (C) HSQC of CM-QAOC (F1: chemical shift of ^{13}C; F2: chemical shift of ^{1}H).

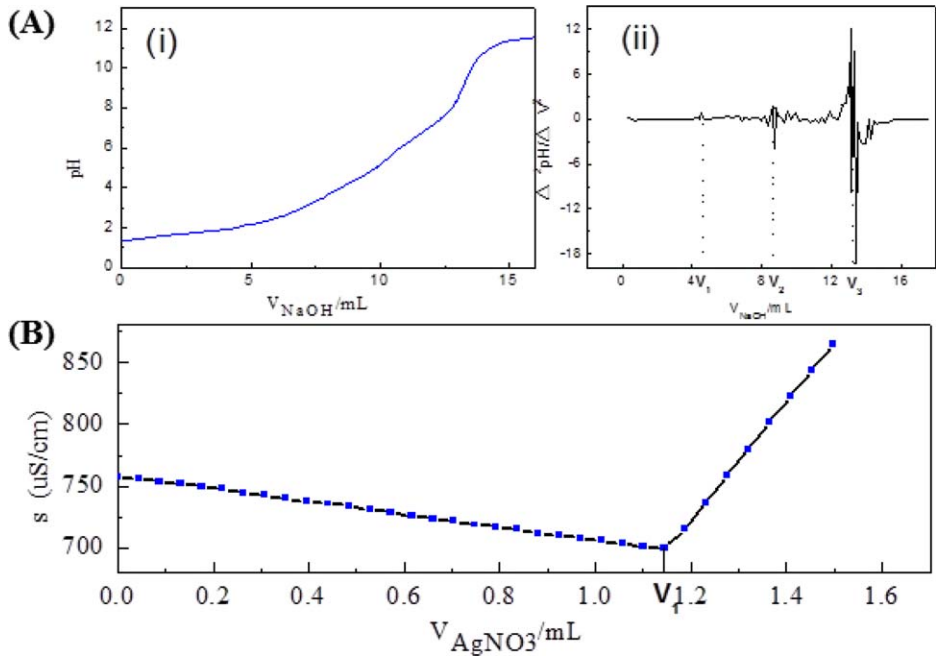

Figure 3. Titration results for the determination of the degree of substitution: (A-i) potentiometric titration curve, (A-ii) second partial derivative calculation, and (B) complexometric titration curve (V_{NaOH}: the consumption volume of NaOH solution; V_{AgNO3}: the consumption volume of $AgNO_3$ solution). [Color figure can be viewed in the online issue, which is available at wileyonlinelibrary.com.]

redundant HCl, $V_{2,NaOH}$ reveals the volume of NaOH titrant consumed by redundant HCl and —COOH, and $V_{3,NaOH}$ reveals the volume of NaOH titrant consumed by redundant HCl, —COOH, and —NH_2. Calculated with eq. (1), DSC was 1.04. In view of the titration diagram shown in Figure 3(B), $V_{1,AgNO3}$ is the titrant volume of the $AgNO_3$ solution at the minimum conductivity, and as calculated according to the eq. (2), the DSQ value was 0.75.

Evaluation of the Scale Inhibition Performances

Conductivity Method. It is well known that nucleation is the first step in precipitation, and this holds true for the scaling deposit as well. *S* is a key point in homogeneous nucleation. When the ion product is beyond this point, the homogeneous nucleation rate increases suddenly, and this results in precipitation and scaling. So, the antiscaling efficiency can be evaluated by S_r, which is expressed as the ratio of S_p to the value of S_0. The higher the S_r value is, the harder it is to form a precipitate. As a result, the scale inhibition efficiency is better.[40]

With regard to this study, the diagram in Figure 4(A) shows the titration results of the solutions containing different dosages of scale inhibitor at 30°C. In the absence of CM-QAOC, the titration volume of Na_2CO_3 when the conductivity suddenly

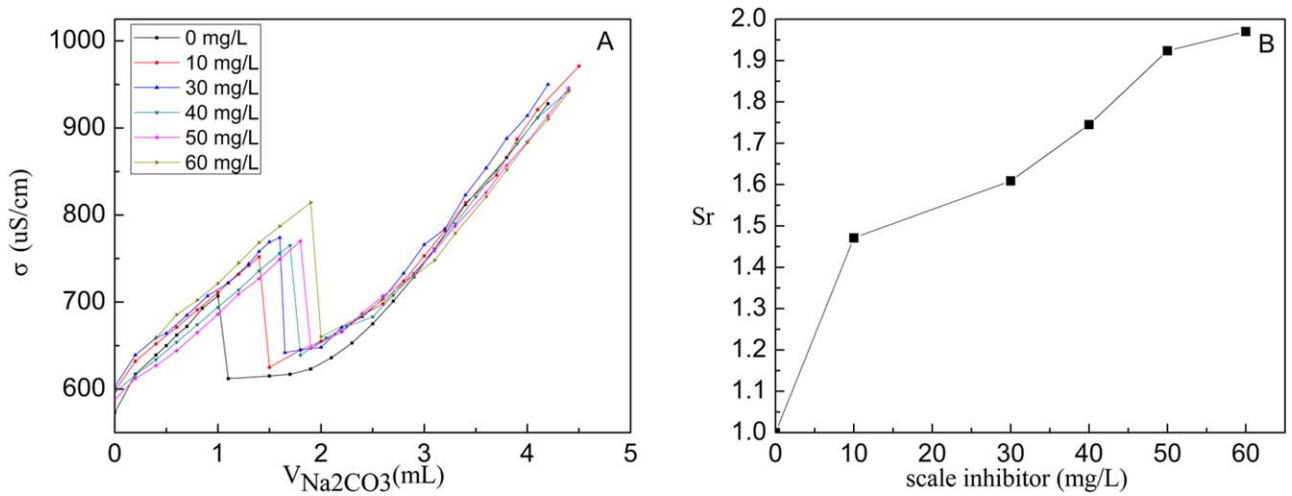

Figure 4. (A) Titration diagram for solutions in the presence and absence of a scale inhibitor and (B) dependence of S_r of $CaCO_3$ on the concentration of the scale inhibitor ($V_{Na_2CO_3}$: titration volume of Na_2CO_3 solution). [Color figure can be viewed in the online issue, which is available at wileyonlinelibrary.com.]

Table I. Effects of the CM-QAOC Dosage on the Scale Inhibition Ratio

CM-QAOC dosage at pH 8.0 (mg/L)	Scale inhibition ratio (%)
10	70.2
30	74.8
40	87.2
50	98.5
60	98.7

decreased was 0.85 mL, as shown in the diagram. At this critical point, solution opalescence was noticed, and a rapid $CaCO_3$ precipitation appeared simultaneously, meanwhile, the conductivity decreased rapidly within a few minutes. A linear relationship between the conductivity and concentration was shown again with further titration. In the presence of CM-QAOC at a concentration of 50 mg/L, solution opalescence was noticed at a titration volume of 0.85 mL but without the occurrence of precipitation until the titration volume was 2.0 mL. So, the boundary volume of Na_2CO_3 consumption was 2.0 mL. According to eq. (3), the values of S_0 and S_p of 50 mg/L CM-QAOC were 895 and 1722, respectively. There was an apparent difference in S when CM-QAOC was present and absent; this implied that CM-QAOC inhibited the carbonate scales very effectively.

The dependence of S_r on the concentration of CM-QAOC is presented in Figure 4(B). As shown in Figure 4(B), S_r increased with an increasing dosage of CM-QAOC. When the concentration of CM-QAOC was above 50 mg/L, a further increase in the dosage caused a smaller increase in S_r. Thus, the optimal dosage of CM-QAOC was 50 mg/L as the scale inhibition efficiency showed no significant improvement exceeding this value.

In conclusion, the conductivity method showed that calcium carbonate scales could be inhibited very effectively by CM-QAOC, with the optimal dosage being 50 mg/L. The excellent carbonate scale inhibition performance was probably due to the fact that CM-QAOC could make the crystal particles disperse, and the solubility of calcium carbonate increased; this caused an increase in S of calcium carbonate. As a result, the precipitation progress was inhibited at the nucleation step.

Static Antiscaling Method. Many factors influence the scale inhibition efficiency, including the dosage of scale inhibitor, Ca^{2+} concentration, pH value, experimental temperature, and duration. In this study, various experiments were designed to study the impact of the inhibitor dosage and pH values on the antiscaling performances.

The effect of the CM-QAOC dosage on the scale inhibition efficiency to $CaCO_3$ scales is shown in Table I. The results indicate that the scale inhibition ratio rose dramatically with an increasing dosage of CM-QAOC from 10 to 50 mg/L. The scale inhibition ratio was reached above 98% when the dosage of CM-QAOC was 50 mg/L with a Ca^{2+} concentration of 240 mg/L and remained stable above 50 mg/L. In addition, the variation of the scale inhibition ratio shown in Table I followed a similar trend to the relative change of supersaturation shown in Figure 4(B); this indicated that these two appraisal methods are consistent.

CM-QAOC contains carboxyl, hydroxyl, and amino groups. These active groups could bind Ca^{2+} to form chelates in solution, which could be adsorbed on the surfaces of the scales. The bonding strength disordered the normal lattice structure of the calcium carbonate crystals; this was helpful for scaling to dissolve to Ca^{2+}. With increasing inhibitor dosage, the number of bonds formed between the inhibitor and Ca^{2+} increased too; this resulted in an improvement in the inhibition efficiency.[41,42] When the concentration of the inhibitor was beyond the optimal value, the inhibitor exhibited an obvious threshold effect; this meant that when the concentration of the scale inhibitor exceeded a certain value (50 mg/L in this study), the inhibition efficiency did not increase obviously.[43]

The comparisons of the scale inhibition between CM-QAOC and some other green scale inhibitors are listed in Table II.[32,42,44–47] From the table, one can see that CM-QAOC had a

Table II. Comparison of CM-QAOC's Scale Inhibition Efficiency with Other Scale Inhibitors

Scale inhibitor	Total calcium (mg/L)	Inhibition efficiency (%)	Concentration (mg/L)	Reference
CM-QAOC	240	98.5	50	
Copolymer modified chitosan	240	95.62	200	44
Poly(epoxysuccinic acid)	500	>95	31.2	42
Poly(aspartic acid)	500	80	12	32
Collagens modified by multialdehyde acid compounds				45
1	250	61	35	
2	—	78	—	
3	—	93	—	
4	—	89	—	
Fig leaf extract	—	85	75	46
Low-phosphorus maleic acid and sodium ρ-styrene sulfonate copolymer	98	98.56	16	47

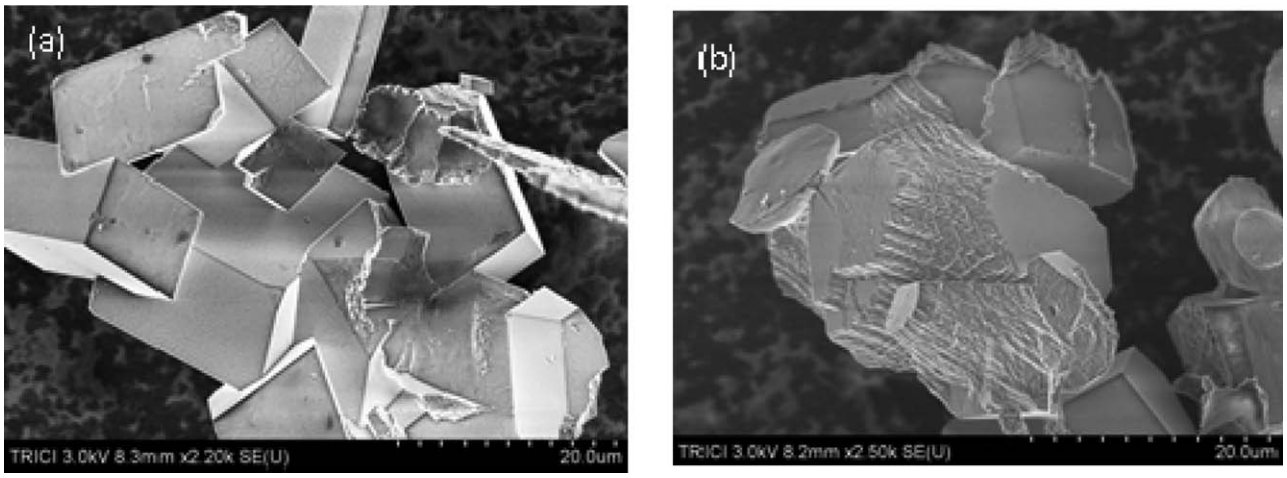

Figure 5. SEM pictures of $CaCO_3$ (a) without and (b) with CM-QAOC.

better scale inhibition efficiency but a far lower optimal concentration than a maleic anhydride–styrene sulfonic sodium–acrylic amide polymer modified chitosan and fig leaf extract[44,46] and a similar inhibition efficiency to modified collagens and polyepoxysuccinic acid but a little higher optimal concentration.[42,45] The reason was probably that CM-QAOC had more groups and a more advantageous configuration but less crosslinking structures than the polymer-modified chitosan or collagens for binding with the scaling components. In addition, because quaternary ammonium is a cationic group, which is beneficial for chitosan to be adsorbed on $CaCO_3$ crystal particles for inhibiting the growth of crystals, CM-QAOC was better than the polymer-modified chitosan and some other green polymer scale inhibitors. At the same time, it had a lower inhibition efficiency and a higher optimal concentration than the phosphorous polymer scale inhibitor.[47] However, with regard to eutrophication caused by phosphorous polymers and the refractory of other synthetic polymers, CM-QAOC is a promising antiscalant.

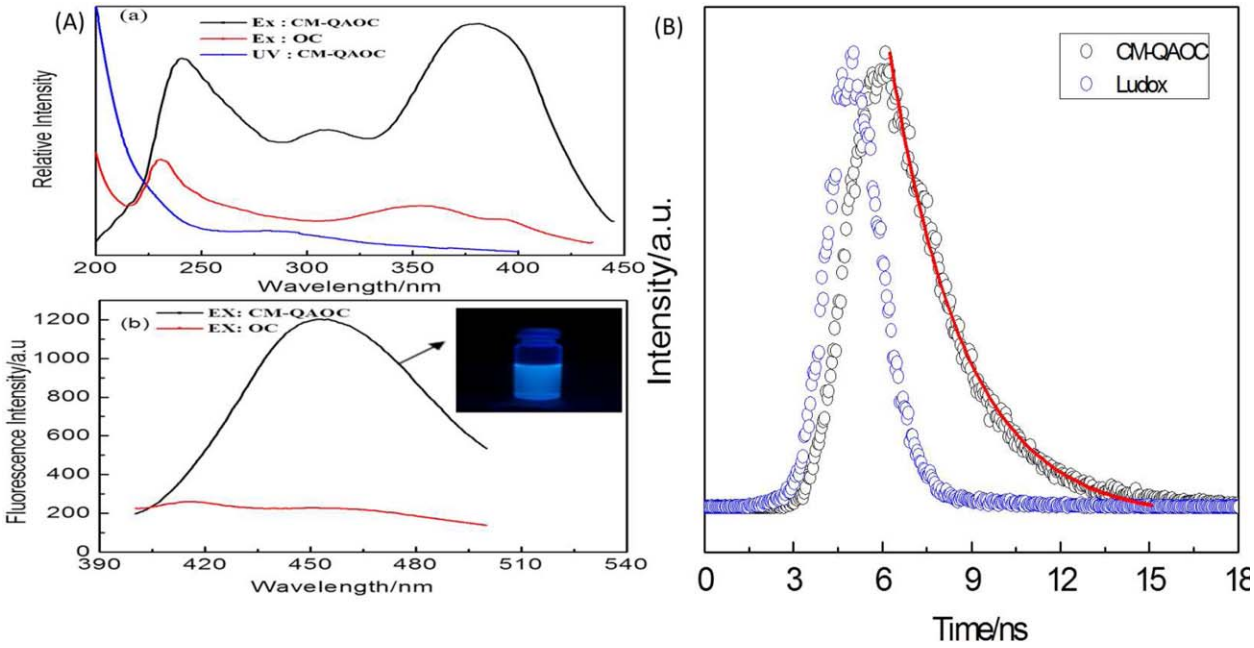

Figure 6. (A) Fluorescence spectra of OC (red) and CM-QAOC (black) and UV–vis spectra of CM-QAOC (blue) at a concentration of 50 mg/L in H_2O: (a) excitation spectra emitted at 460 nm (Ex: the excitation spectra when the emission wavelength was 460 nm) and (b) emission spectra excited at 380 nm (EX: the emission spectra when the excitation wavelength was 380nm). The blue emission came from CM-QAOC under 365-nm irradiation. (B) Decay curves of CM-QAOC: (○) experimental curve and (-) curve fitted according to $I = I_0 + A \exp[-(t - t_0)/\tau]$. (I: the fluorescence intensity when t=t; I_0: the fluorescence intensity when $t=t_0$; A: the amplitude of the fitted function; t: time; τ: fluorescence lifetime) For the interpretation of the references to color in this figure legend, the reader is referred to the Web version of this article. [Color figure can be viewed in the online issue, which is available at wileyonlinelibrary.com.]

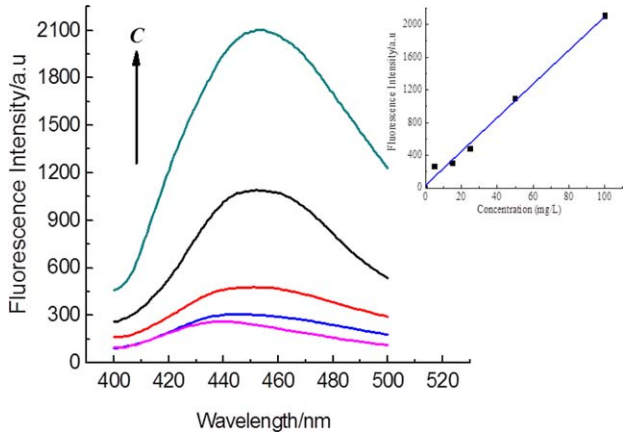

Figure 7. Emission spectra of CM-QAOC at different concentrations in H_2O. The wavelength of excitation was 380 nm. The inset shows the calibration curve. [Color figure can be viewed in the online issue, which is available at wileyonlinelibrary.com.]

SEM Pictures of the Calcium Carbonate Scale. To obtain a better understanding of the impact of CM-QAOC on $CaCO_3$ crystallization, the $CaCO_3$ crystals scaling from the static anti-scaling experiments were collected and observed by means of SEM. As shown in Figure 5, without CM-QAOC, the $CaCO_3$ crystals showed a calcite structure with a glossy surface, a regular shape, and a compact structure [Figure 5(a)]. On the other hand, after CM-QAOC was added, the resulting $CaCO_3$ scale displayed irregular and cascade patterns with obvious floppy accumulation [Figure 5(b)]. On basis of the analyses for the SEM diagram, we speculated that the functional groups, such as carboxylate, hydroxyl, and amino groups, had chelating and dispersion abilities to the metal ions; this interfered with the formation of crystals, and the growth of the crystalline cold not be in strict accordance with the normal lattices; at last, irregular shapes (flowers and cascades) appeared in loose structures.[48] Consequently, the scales could be washed away freely with water.

Fluorescence Properties of CM-QAOC

Figure 6(A) shows the excitation and emission fluorescence spectra of CM-QAOC and OC. CM-QAOC presented two excitation bands at 250 and 380 nm and an emission band at 450 nm. In comparison with CM-QAOC, OC showed very weak fluorescence bands. These results indicate that some special fluorescent components or favorite configurations appeared in the structure of CM-QAOC. The reasons for this may have been the introduction of some functional groups, such as carboxyl or quaternary ammonium groups. These functional groups can achieve an $n\rightarrow\pi^*$ transition by p–π conjunction between —C═O and —NH—; this is the precondition of fluorescence in these molecules. Furthermore, hydrogen bonding, which can make the molecular structure rigid, could be formed between —C═O and —NH—. With the existence of quaternary ammonium groups, the charge–charge repulsion could cause molecular expansion and make the functional groups crowded; this tended to make the molecules form a dense network structure. In acidic conditions, the secondary amine could be protonated, and this could make the molecules more crowded. So, we deduced that the fluorescence intensity was stronger under acidic conditions. Thus, in one word, the hydrogen bonding and the charge–charge repulsion made a rigid and densely stabilized structure, which is necessary for inducing fluorescence. Hence, the fluorescence of CM-QAOC may have been caused by the effect of the $n\rightarrow\pi^*$ transition between —C═O and —NH— and the special rigid structure formed by hydrogen bonding and charge–charge repulsion.[49]

Furthermore, in the absorption spectrum of CM-QAOC, there were no correlation absorption bands appearing at the positions of the excitation bands. The phenomenon of weak absorption but strong fluorescence is rare in organic luminescent compounds. The absence of conjugated structures on the polymer may account for the low absorptivity. Similar fluorescence phenomenon is also observed from NH_2-terminated, OH-terminated, and carboxylate-terminated polyamidoamine dendrimers and from NH_2-terminated polypropylene imine dendrimers.[49,50]

In time-resolved measurements, the fluorescence decay of CM-QAOC was fitted well by a single-exponential function [Figure 6(B)]; the lifetime was determined to be 1.91 ns, and χ^2 (Goodness of Fit) was 1.006. This indicated that it was reasonable to determine that CM-QAOC had one fluorescence lifetime. The lifetime was similar to that of Rhodamine B (1.75 ns in a water solution), a common reagent used in fluorescence tracer, and the second lifetime of G-5.5-carboxylate-terminated polyamidoamine (1.91 ns in methanol).[49,51]

This fluorescent properties showed the unique aspects of CM-QAOC and could probably be used in its characterization and tracing applications. During the fluorescent quantitative analysis that is necessary for the tracer technology to determine the water-treatment chemical concentration, the fluorescence intensity should be proportional to the concentrations of the samples and should exhibit good reproducibility. In our experiments, the relationship between the fluorescence intensity and the concentration of CM-QAOC was investigated. The emission spectra of CM-QAOC (with concentrations of 5, 15, 25, 50, and

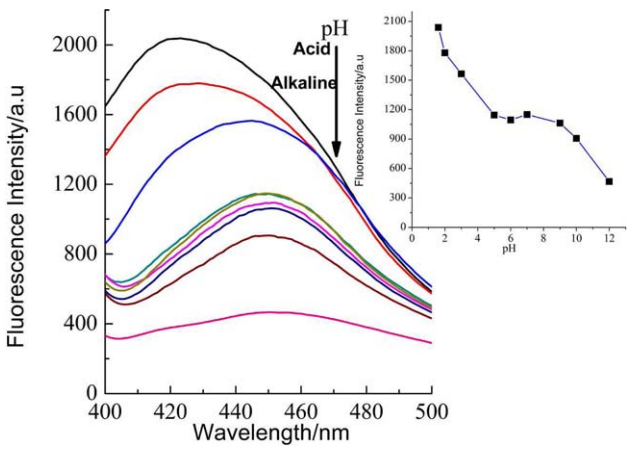

Figure 8. Fluorescence emission spectra of CM-QAOC (50 mg/L) at different pH values. The inset shows the pH-dependent fluorescence intensity. [Color figure can be viewed in the online issue, which is available at wileyonlinelibrary.com.]

100 mg/L) were measured with an excitation wavelength of 380 nm. As shown in Figure 7, the results indicate that the fluorescence intensity increased with increasing CM-QAOC concentration from 5 to 100 mg/L. A good linear relationship was presented between them, and the correlation coefficient was significant at 0.99. The detection limit of CM-QAOC ($3\sigma/\kappa$, σ is the variance and κ is the slope)[52] was obtained at 0.6046 mg/L when the CM-QAOC concentration was in the range 5–100 mg/L. So, the fluorescent quantitative analysis was achieved and could be used to detect the concentration of CM-QAOC in H_2O. Therefore, CM-QAOC could be used not only as a scale inhibitor but also as a tracer, and on top of that, it was a kind of self-traced agent to determine its own concentration with the fluorescence induced by itself.

The changes of the fluorescent properties of CM-QAOC in a phosphate buffer solvent at different pH values are depicted in Figure 8. As shown in Figure 8, CM-QAOC showed significant pH-dependent fluorescence properties in the pH range from 12 to 1.5. The emission intensity rapidly increased with decreasing pH values from 5 to 1.5. When the pH decreased from 9 to 5, there was little change in the emission intensity. However, when the pH was above 9, a rapid decrease in the fluorescence intensity appeared again. The emission band position was scarcely changed in the pH range from 12 to 5, whereas it showed a blueshift from 450 to 423 nm in the pH range from 5 to 1.5. Some assumptions can be provided to explain the previous phenomenon: (1) below pH 5, the protonation of amine and carboxyl groups filled the whole reticular interior with cations, and the strong charge–charge repulsion made the structure of CM-QAOC more rigid, and (2) the strength of hydrogen bonds in the CM-QAOC structure was enhanced under acidic conditions; this could also account for the blueshift of the fluorescence spectra.[53,54] It is common that industrial recirculated cooling water is likely neutral or weakly alkalinic, with a pH value of 7–9. Thus, it can be suggested that when CM-QAOC is used in industrial recirculated cooling water systems, the fluorescence intensity and emission band position will scarcely change under normal routine operations. If the fluorescence intensity weakens, this would imply that an agent in the water system is probably needed because it has been consumed or the water chemistry has changed to be corrosive ($pH < 5$) or easily scaled ($pH > 9$) in the water system.

CONCLUSIONS

CM-QAOC was prepared successfully from depolymerized chitosan via carboxymethylation and quaternization. CM-QAOC had excellent inhibition ability against $CaCO_3$ scaling, as evaluated by the conductivity method and static test. With a Ca^{2+} concentration of 240 mg/L, a pH value of 8.0, and a CM-QAOC dosage of 50 mg/L, the inhibition ratio for calcium carbonate scaling reached above 98%. The SEM images showed that the calcium carbonate scale was porous and floppy in the presence of CM-QAOC, and the scales could easily flow away with water. In addition, we found that CM-QAOC was possessed of detectable fluorescence with the introduction of carboxymethyl and quaternary ammonium groups. The fluorescence intensities accorded well with the concentrations of CM-QAOC with the detection limit of 0.6046 mg/L; the fluorescence intensity was constant at pH 5–9, while it showed apparent changes out of this pH range. This interesting phenomenon has not been reported by other researchers as far as we know, and its novel fluorescent properties could make this an excellent scale inhibitor furnished with built-in or latent self-traced and tracing functionalities without any further modification or composition with any fluorescent groups or agents. To better gauge its functional tracing potential, its fluorescent properties and compatibilities with other water-treatment chemicals under various conditions in water systems should be studied in further research. In addition, the fluorescence mechanism should also be studied seriously in future research.

ACKNOWLEDGMENTS

Part of this work was supported by the National Natural Science Foundation of China (contract grant numbers 21171046 and 21271060). The authors thank Ke Lu for assistance with the measurements of the fluorescence properties.

REFERENCES

1. Xu, Y.; Zhao, L. L.; Wang, L. N.; Xu, S. Y.; Cui, Y. C. *Desalination* **2012**, *286*, 285.
2. Abdel-Aal, N.; Sawada, K. *J. Cryst. Growth* **2003**, *256*, 188.
3. Dyer, S. J.; Anderson, C. E.; Graham, G. M. *J. Pet. Sci. Eng.* **2004**, *43*, 259.
4. Hasson, D.; Shemer, H.; Sher, A. *Ind. Eng. Chem. Res.* **2011**, *50*, 7601.
5. Touir, R.; Dkhireche, N.; Ebn Touhami, M.; Lakhrissi, M.; Lakhrissi, B.; Sfaira, M. *Desalination* **2009**, *249*, 922.
6. De Souza, F. S.; Spinelli, A. *Corros. Sci.* **2009**, *51*, 642.
7. Hoots, J. E.; Hunt, B. E. U.S. Pat. 4,783,314 (**1988**).
8. Hoots, J. E. U.S. Pat. 5,171,450 (**1992**).
9. Moriarty, B. E.; Reddinger, J. L. U.S. Pat. 6,358,746 (**2002**).
10. Moriarty, B. E.; Morris, J. D.; Murray, P. G.; Reddinger, J. L.; Wei, M. L. U.S. Pat. 7,875,720 (**2011**).
11. Moriarty, B. E.; Bakalik, D. P.; Davis, R. V.; Hoots, J. E.; Shiely, R. W. U.S. Pat. 6,280,635 (**2001**).
12. Simionescu, C. L.; Percec, V. *J. Polym. Sci. Polym. Chem. Ed.* **1979**, *17*, 2287.
13. Sashima, H.; Kawasaki, N.; Nakayama, A.; Muraki, E.; Yajima, H.; Yamamori, N.; Ichinose, Y.; Sunamoto, J.; Aiba, S. *Carbohydr. Res.* **2003**, *338*, 557.
14. Grini, G.; Badot, P. M. *Prog. Polym. Sci.* **2008**, *33*, 399.
15. Wedmore, I.; McManus, J. G.; Pusateri, A. E.; Holcomb, J. B. *J. Trauma* **2006**, *60*, 655.
16. Li, Q.; Ren, J. M.; Dong, F.; Feng, Y.; Gu, G. D.; Guo, Z. Y. *Carbohydr. Res.* **2013**, *373*, 103.
17. Prashanth, K. V. H.; Tharanathan, R. N. *Trends Food Sci. Technol.* **2007**, *18*, 117.
18. Schmuhl, S.; Krieg, H. M.; Keizer, K. *Water SA* **2001**, *27*, 1.
19. Dambies, L.; Vincent, T.; Guibal, E. *Water Res.* **2002**, *36*, 3699.

20. Hall, L. D.; Yalpani, M. *Carbohydr. Res.* **1980**, *83*, C5.
21. Cano-Cebrian, M. J.; Zornoza, T.; Granero, L.; Polache, A. *Curr. Drug Delivery* **2005**, *2*, 9.
22. Xu, Y. M.; Du, Y. M.; Huang, R. H.; Gao, L. P. *Biomaterials* **2003**, *24*, 5015.
23. Mao, S.; Shuai, X. T.; Unger, F.; Simona, M.; Bi, D. Z.; Kissel, T. *Int. J. Pharm.* **2004**, *281*, 45.
24. Maghami, G. G.; Roberts, G. A. F. *Makromol. Chem.* **1988**, *189*, 195.
25. Cerrutti, B. M.; Lamas, J. C.; Campana-Filho, S. P.; Frollini, E. *J. Polym. Environ.* **2013**, *21*, 816.
26. Zhang, H. X.; Ge, L. H.; Zhou, H. Y.; Zhu, Y. C.; Wang, F. *Chem. Ind. Eng. Prog.* **2011**, *30*, 2055.
27. Seong, H. S.; Whang, H. S.; Ko, S. W. *J. Appl. Polym. Sci.* **2000**, *76*, 2009.
28. Li, X. F.; Feng, X. Q.; Yang, S. *Food Sci.* **2010**, *31*, 76.
29. Li, H. B.; Du, Y. M.; Wu, X. J.; Zhan, H. Y. *Colloids Surf. A* **2004**, *242*, 1.
30. Drela, I.; Falewicz, P.; Kuczkowska, S. *Water. Res.* **1998**, *32*, 3188.
31. Gu, X. X.; Qiu, F. X.; Zhou, X.; Qi, J.; Zhou, Y.; Yang, D. Y.; Guo, Q.; Guo, X. R. *Int. J. Polym. Mater.* **2013**, *62*, 323.
32. Liu, D.; Dong, W. B.; Li, F. T.; Hui, F.; Lédion, J. *Desalination* **2012**, *304*, 1.
33. Li, P. C.; Xing, R.; Liu, S.; Yu, H. H. U.S. Pat. 7,648,969 (**2010**).
34. Chen, X. G.; Park, H. *J. Carbohydr. Polym.* **2003**, *53*, 355.
35. Sangeetha, Y.; Meenakshi, S.; SairamSundaram, C. *Int. J. Biol. Macromol.* **2015**, *72*, 1244.
36. Qin, C. Q.; Xiao, Q.; Li, H. R.; Fang, M.; Liu, Y.; Chen, X. Y.; Li, Q. *Int. J. Biol. Macromol.* **2004**, *34*, 121.
37. Chen, L. Y.; Du, Y. M.; Zeng, X. Q. *Carbohydr. Res.* **2003**, *338*, 333.
38. Rinaudo, M.; Dung, P. L.; Gey, C.; Milas, M. *Int. J. Biol. Macromol.* **1992**, *14*, 122.
39. Ning, Y. C. Structural Identification of Organic Compounds with Spectroscopic Techniques; Wiley-VCH: Weinheim, **2005**; Chapter 4.
40. Chen, T.; Neville, A.; Yuan, M. D. *J. Pet. Sci. Eng.* **2005**, *46*, 185.
41. Kumar, T.; Vishwanatham, S.; Kundu, S. S. *J. Pet. Sci. Eng.* **2010**, *71*, 1.
42. Zhou, X. H.; Sun, Y. H.; Wang, Y. Z. *J. Environ. Sci.* **2011**, *23*, S159.
43. Tang, Y. M.; Yang, W. Z.; Yin, X. S.; Liu, Y.; Yin, P. W.; Wang, J. T. *Desalination* **2008**, *228*, 55.
44. Guo, X. R.; Qiu, F. X.; Dong, K.; Zhou, X.; Qi, J.; Zhou, Y.; Yang, D. Y. *J. Ind. Eng. Chem.* **2012**, *18*, 2177.
45. Qiang, X. H.; Sheng, Z. H.; Zhang, H. *Desalination* **2013**, *309*, 237.
46. Abdel-Gaber, A. M.; Abd-El-Nabey, B. A.; Khamis, E.; Abd-El-Khalek, D. E. *Desalination* **2008**, *230*, 314.
47. Wang, C.; Zhu, D. Y.; Wang, X. K. *J. Appl. Polym. Sci.* **2010**, *115*, 2149.
48. Gopi, S. P.; Vijaya, P.; Subramanian, V. K. *Powder Technol.* **2012**, *225*, 58.
49. Larson, C. L.; Tucker, S. A. *Appl. Spectrosc.* **2001**, *55*, 679.
50. Wang, D. J.; Imae, T. *J. Am. Chem. Soc.* **2004**, *126*, 13204.
51. Zhang, X. F.; Zhang, Y. K.; Liu, L. M. *J. Lumin.* **2014**, *145*, 448.
52. Xie, A. J.; Luo, S. P.; Wu, W. Z. *Chin. J. Spectrosc. Lab.* **2012**, *29*, 1609.
53. Malyarenko, D. I.; Vold, R. L.; Hoatson, G. L. *Macromolecules* **2000**, *33*, 1268.
54. Xu, J. G.; Wang, Z. B. Fluorescence Analysis, 3rd ed.; Science: Beijing, **2006**; Chapter 3.